PHYSICAL REVIEW B VOLUME 19, NUMBER 2 15 JANUARY 1979

Reconstruction of momentum distribution from point-geometry positron-annihilation data

L. Pecora and A. C. Ehrlich
Material Science and Technology Division, Naval Research Laboratory, Washington, D.C. 20375
(Received 8 May 1978)

A method is presented by which the momentum distribution of the electrons in a metal, $\rho(\vec{p})$, may be reconstructed from point-geometry angular-correlation positron-annihilation data taken in a plane. The result is in the form of a truncated Fourier series in polar coordinates in that plane in momentum space. The number of terms in the $\rho(\vec{p})$ series is determined by the number of crystal orientations at which data were taken. The effect of statistical errors in the data on the reconstruction of $\rho(\vec{p})$ is examined for a hypothetical free-electron metal. The method is applied to real data taken in the (100) plane of Cu, and it is found that the comparison to the theoretically predicted $\rho(\vec{p})$ is remarkably good. In particular, the results show that surprisingly rich detail in $\rho(\vec{p})$ can be reproduced using data taken for a minimum number of crystal orientations.

I. INTRODUCTION

In positron annihilation or Compton-profile scattering the object of study is the momentum distribution function $\rho(\vec{p})$ of the electrons in the material being examined. However, neither experimental method enables one to directly measure $\rho(\vec{p})$. Insufficient resolution of Doppler shifts in available experimental apparatus leads to each measurement being an integral over $\rho(\vec{p})$ along the momentum axis parallel to the collimating apparatus. Often, by choice (e.g., the long-slit positron-annihilation apparatus), the measured data consists of two integrations over $\rho(\vec{p})$, thus

$$N(p_z)=\int_{-\infty}^{\infty}\int_{-\infty}^{\infty} dp_x\,dp_y\,\rho(\vec{p})\,, \tag{1}$$

where $N(p_z)$ is the number of coincidence counts at momentum p_z.

The situation in which one wishes to obtain a function defined on a two- or three-dimensional domain from values of its integrals over lines or planes, respectively, is encountered in many fields. Reconstruction of the function by calculation of its two- or three-dimensional Fourier transform has been shown to be feasible by a number of workers in various areas.[1-3] Other methods[1,4-6] for reconstruction have included expansion of the unknown function in various polynomials or sets of functions, such as cylinder functions. The expansion coefficients are then obtained by solving the equations which are generated from the relationship between the data and the desired function [Eq. (1), for example]. Mijnarends' expansion[6] in terms of Kubic harmonics is the three-dimensional analog of our method and has been used by a number of workers in positron annihilation.[7-9] Because of this, throughout this paper, we shall compare our two-dimensional results using point-geometry data with the three-dimensional results using long-slit data obtained using his method. A solution to the two-dimensional problem which is encountered in radiology was given by Cormack[10,11] and is mathematically equivalent to ours. The comparison of our work and Cormack's will be covered in more detail later in this paper. Finally two very good reviews of the general reconstruction problem and its practical solutions are given by Cormack[12] and Brooks and deChiro.[13]

The method of Mijnarends[1] consists of expanding $\rho(\vec{p})$ in terms of Kubic harmonics appropriate for the crystal symmetry and solving the integral equation which results from insertion of this expansion in Eq. (1). In general a good approximation to $\rho(\vec{p})$ is obtained only for sets of data taken at many different directions, usually six or more. For reasons of geometry the long-slit method does not yield an accurate reconstruction of $\rho(\vec{p})$ near $\vec{p}=0$,[7] although the functionality of $\rho(\vec{p})$ near $\vec{p}=0$ can be determined from an analysis of the curvature of the profile near zero momentum.[14] However, the very nature of Eq. (1) requires us to reconstruct $\rho(\vec{p})$ for all p values, which requires a great deal of information. This accounts for the restrictions on the accuracy of the long-slit reconstruction results.

The drawbacks to the long-slit method just mentioned can be circumvented to a great extent by the use of the point geometry or, so called, crossed-slit setup for positron annihilation. In this setup collimation of the emitted γ rays is done in two directions and thus two components of momenta can be resolved simultaneously. Mathematically this means that the data can be expressed as a single integral of $\rho(\vec{p})$ over the momentum parallel to the γ rays which, as mentioned, cannot be resolved. Usually, one of the two resolved components is held constant (usually

zero) while the other is varied. Thus we express the data as follows:

$$N_\alpha(p_z)=\int_{-\infty}^{\infty} dp_x\,\rho(p,p_y=0)\,, \tag{2}$$

where p_z is the component of momenta of the positron-electron pair at which coincidence counts are being taken, p_x is the component of momenta parallel to the γ rays, and α is the angle between a fixed direction (such as a major symmetry direction) in the p-space plane, defined by $p_y=0$, and p_z, i.e., α determines the orientation of the apparatus coordinate system with respect to the fixed crystal coordinate system. Because of the nature of Eq. (2) it will prove possible to reconstruct $\rho(\vec{p})$ in the given plane in extended p space from data, $N_\alpha(p_z)$, taken for various crystal orientations in that plane. This means that less information will be required to reconstruct the restricted function $\rho(\vec{p},p_y=0)$ than would be required to reconstruct the full $\rho(\vec{p})$ function. Thus we should get better results near $\vec{p}=0$ and better results overall with experimental runs taken at fewer directions than are necessary for the long-slit analysis. Although $\rho(\vec{p})$ will be determined only in a specified $\vec{p}$-space plane and not over all $\vec{p}$ space, this will not generally be a severe limitation since one is usually interested only in specific directions which often lie in just one or two planes.

In Sec. II we develop an approximation for the point-geometry setup in a manner analogous to Mijnarends' method for the long-slit data. In Sec. III the method is tried on hypothetical free-electron-plus-Gaussian-core data and the effect of data-point errors in the reconstruction of $\rho(\vec{p})$ is examined. Finally in Sec. IV the method is applied to real data taken in the (001) p-space plane of Cu. The results are compared to theoretical expectations for $\rho(p)$ in the [100] and [110] directions in p space.

II. THEORY

We assume that $p_y=0$ so that the data taken represent integrations of $\rho(\vec{p})$ in the plane in $\vec{p}$ space defined by $p_y=0$. Further, let α_j be the angle of the orientation of the experimental apparatus with a fixed direction ζ in the crystal $p_y=0$ plane. The data points $N_{\alpha_j}(p_z)$ then represents integrals of $\rho(\vec{p},p_y=0)$ over lines in the $p_y=0$ plane whose perpendicular distance to the origin is p_z and whose angle of orientation is α_j. Figure 1 shows this schematically. Thus for each α_j we have a set of data for various p_z, $[N_{\alpha_j}(p_z)\,|-\infty<p_z<\infty]$. The full set of data is the totality of the data sets for all α_j, $j=1,2,3\ldots,n$.

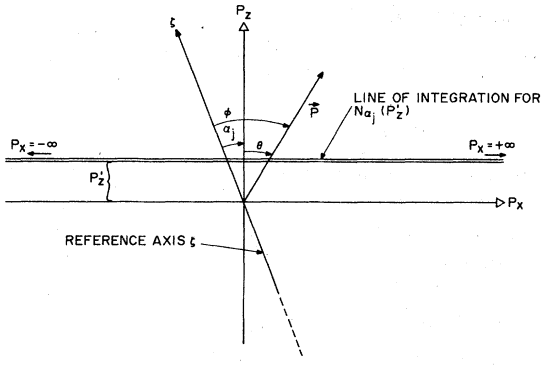

FIG. 1. Extended k-space plane of integration for Eq. (2). ζ is a fixed crystallographic direction and the p_xp_z axes represent the coordinate system of the experimental apparatus. The double line represents a typical integration direction at a value of $p_z=p'_z$ so that the data generated would be represented by $N_\alpha(p'_z)$.

Since $\rho(\vec{p})$ will only be defined in a plane we may expand it in a Fourier series in polar coordinates

$$\rho(\vec{p})=\sum_{m=-\infty}^{m=+\infty}\rho_m(p)e^{im\phi}\,, \tag{3}$$

where $p\equiv|\vec{p}|$ and ϕ is the angle of $\vec{p}$ with respect to the reference direction in the plane (see Fig. 1). The coefficients $\rho_m(p)$ are not completely arbitrary since $\rho(\vec{p})$ must be real. This yields the conditions

$$\mathrm{Re}[\rho_m(p)]\equiv\rho^r_m(p)=\rho^r_{-m}(p)\,,$$

$$\mathrm{Im}[\rho_m(p)]\equiv\rho^i_m(p)=-\rho^i_{-m}(p)\,.$$

Hence we can restrict ourselves to solving for coefficients $\rho_m(p)$ for which $m\geq 0$.

Equation (3) must be integrated along p_x according to Eq. (2). This means we must transform to the p_x-p_z system. This is accomplished by letting

$$\phi=\alpha_j+\theta\,,$$

where $\theta=\arccos(p_z/p)$. This yields

$$\rho(\vec{p})=\sum_{-\infty}^{+\infty}e^{im\alpha_j}\rho_m(p)e^{im\theta}\,. \tag{4}$$

Inserting Eq. (4) into Eq. (2) we have

$$N_{\alpha_j}(p_z)=\sum_{m=-\infty}^{\infty}e^{im\alpha_j}\int_{-\infty}^{\infty}dp_x\,\rho_m(p)\cos m\theta\,, \tag{5}$$

where we have used $e^{im\theta}=\cos m\theta+i\sin m\theta$ and the fact that the integral generated by $\sin m\theta$ is odd in p_x and vanishes. The variables p and θ are no longer independent since the integral is restricted to a straight line in the plane. The integration variable can be changed to p, thus eliminating θ and p_x, as follows. Using the relation

$$p_x=(p^2-p_z^2)^{1/2},$$

we have

$$dp_x=\frac{p\,dp}{(p^2-p_z^2)^{1/2}}.$$

The angular dependence of θ is eliminated by using $\theta=\arccos(p_z/p)$ and $\cos m\theta=T_m(\cos\theta)$. T_m is a Chebychev polynomial of the first kind and is defined by

$$T_m(x)=\cos[m\arccos(x)].$$

Thus $\cos m\theta=T_m(p_z/p)$, and Eq. (5) becomes

$$N_{\alpha_j}(p_z)=\sum_{m=-\infty}^{\infty}2e^{im\alpha_j}\int_{|p_z|}^{\infty}\frac{p\,dp}{(p^2-p_z^2)^{1/2}}\rho_m(p)T_m\left(\frac{p_z}{p}\right). \tag{6}$$

Letting

$$g_m(p_z)=2\int_{|p_z|}^{\infty}\frac{p\,dp}{(p^2-p_z^2)^{1/2}}\rho_m(p)T_m\left(\frac{p_z}{p}\right), \tag{7}$$

we have

$$N_{\alpha_j}(p_z)=\sum_{m=-\infty}^{\infty}g_m(p_z)e^{im\alpha_j}. \tag{8}$$

We see that the full set of data, $[N_{\alpha_j}(p_z)|j=1,2,\ldots n,-\infty<p_z<\infty]$, can be expanded in a Fourier series in a plane using the polar coordinates p_z and α_j, i.e., we can think of $N_{\alpha_j}(p_z)$ as a function of two variables, p_z and α_j.

The problem of reconstructing $\rho(\vec{p})$ becomes one of solving for the functions $g_m(p_z)$ in Eq. (8) and then solving the integral Eq. (7) for $\rho_m(p)$ for $m=0,1,2,\ldots$. These may be treated as two separate problems.

There are a number of ways to solve Eq. (8) for $g_m(p_z)$ given a full set of data $[N_{\alpha_j}]$. If the data points were taken for a large number of α_j's (i.e., n large), then $g_m(p_z)$ may be found by a numerical integration of the Fourier integral

$$g_m(p_z)=\frac{1}{2\pi}\int_0^{2\pi}N_\alpha(p_z)e^{-im\alpha}d\alpha.$$

However, the case is usually that we do not have data in the full data set at enough angles to approximate this integral well. The other possibility is that we may view the set of equations generated by Eq. (8) for $j=1,\ldots,n$ as a set of linear equations for each p_z value with n knowns, $N_{\alpha_j}(p_z)$, and an infinite number of unknowns, $g_m(p_z)$. We may solve for a finite number of $g_m(p_z)$ values by truncating the series in Eq. (8). The $g_m(p_z)$ functions obey the same reality conditions as $\rho_m(p)$ since they are related by Eq. (7). This means that if we have n data sets with $n=2l-1$, where l is some integer, we can solve for the first l $g_m(p_z)$ functions. Very often symmetry considerations will allow us to set some of the $g_m(p_z)$ functions or at least their real or imaginary parts equal to zero. This leads to a distinct advantage over the reconstruction of long-slit data when we only desire $\rho(\vec{p})$ along directions in high-symmetry planes. This can be seen as follows. The criteria for truncating the series expansions of $\rho(\vec{p})$ are to drop higher-l terms in the long-slit reconstruction and higher-frequency terms in the point-geometry reconstruction. The number of terms retained in each case is determined by the number of nonequivalent directions in the crystal in which data was taken. Suppose now we desire $\rho(\vec{p})$ only in the (100) plane of a fcc metal. The amount of detail and in general the accuracy of the reconstruction is determined by the number of terms we can retain in the series expansion. In particular the detail of the reconstruction will depend on the frequency of the angular function in the terms retained. Thus if we want terms up to $\cos 12\phi$, where ϕ is the polar angle in the plane we need the first six terms of a long-slit reconstruction, but we only need the first four terms in the point-geometry reconstruction since the fourfold symmetry of the plane reduces the number of nonzero terms and reduces the number of directions at which data must be taken. The reason for this, of course, is that with the long-slit method we must reconstruct $\rho(\vec{p})$ over its entire three-dimensional domain and although certain terms in the expansion may not contribute higher-frequency terms to the reconstruction in a particular plane they must be retained and cannot be arbitrarily dropped in favor of those contributing higher-frequency terms in that plane. The same arguments apply to any plane of high symmetry.

We are now faced with solving Eq. (7) for $\rho_m(p)$ given $g_m(p_z)$. To do this we use the methodology of Mijnarends.[6] We take the case when m is even. Then $g_m(p_z)$ is an even function since Eq. (7) is even in p_z except for the $T_m(p_z/p)$ factor which is even (odd) as m is even (odd) [for more properties of the g_m functions and for proof of the uniqueness of the solution of Eq. (7) see Ref. 10]. First we take the Fourier transform of Eq. (7),

$$\int_0^{\infty}g_m(p_z)\cos(kp_z)\,dp_z$$

$$=\int_0^{\infty}dp\,\rho_m(p)p\int_{-p}^{p}\frac{dp_z}{(p^2-p_z^2)^{1/2}}T_m\left(\frac{p_z}{p}\right)e^{ikp_z}.$$

Performing the integration involving $T_m(p_z/p)$,[15] we have

$$\int_0^\infty g_m(p_z)\cos(kp_z)dp_z = \pi i^m \int_0^\infty dp\, \rho_m(p) p J_m(kp)\,, \quad (9)$$

where $J_m(kp)$ is the Bessel function of the first kind. The right-hand side of Eq. (9) is just the Hankel transform of $\rho_m(p)$, excluding the πi^m factor. Thus upon taking the inverse Hankel transform we have an expression for $\rho_m(p)$ involving a double integral,

$$\rho_m(p) = \frac{1}{\pi i^m} \int_0^\infty dk\, k J_m(kp) \times \int_0^\infty dp_z g_m(p_z)\cos(kp_z)\,. \quad (10)$$

The order of integration cannot be interchanged in Eq. (10) since the integral over k will not converge. However, using the following property of $g_m(p_z)$,

$$\lim_{p_z \to \infty} g_m(p_z) = 0\,,$$

which follows from Eq. (7), we can integrate the p_z integral by parts. This yields

$$\rho_m(p) = \frac{-1}{\pi i^m} \int_0^\infty dk\, J_m(kp) \int_0^\infty \frac{dg_m(p_z)}{dp_z} \sin(kp_z)dp_z\,.$$

The order of integration can now be interchanged and the k integration can be performed.[15] Thus for m even we have an expression for $\rho_m(p)$,

$$\rho_m(p) = \frac{-1}{\pi} \int_0^\infty dp_z \frac{dg_m(p_z)}{dp_z} \begin{cases} \dfrac{(-1)^{m/2}\sin[m \arcsin(p_z/p)]}{(p^2 - p_z^2)^{1/2}}\,, & p_z < p \\ \dfrac{p^m}{(p_z^2 - p^2)^{1/2}[p_z + (p_z^2 - p^2)^{1/2}]^m}\,, & p_z > p\,. \end{cases} \quad (11)$$

A similar analysis for m odd results in

$$\rho_m(p) = \frac{-1}{\pi} \int_0^\infty dp_z \frac{dg_m(p_z)}{dp_z} \begin{cases} \dfrac{(-1)^{(m+1)/2}\cos[m \arcsin(p_z/p)]}{(p^2 - p_z^2)^{1/2}}\,, & p_z < p \\ \dfrac{-p^m}{(p_z^2 - p^2)^{1/2}[p_z + (p_z^2 - p^2)^{1/2}]^m}\,, & p_z > p\,. \end{cases} \quad (12)$$

The p_z integration will be numerical since, in general, $g_m(p_z)$ is known only at a finite number of points. This is no problem in treating positron-annihilation data even though the upper limits of integration are infinite. This is because, to a very good approximation, the data, $N_\alpha(p_z)$, fall off as exponential functions beyond some p_z value. Because of the linear relation between $[N_{\alpha_j}(p_z)]$ and $[g_m(p_z)]$ this means that the $g_m(p_z)$ behave similarly and can either be extended by fitting an exponential to the "tail end" of the function or can be truncated if the values at large p_z are small enough that their contributions to the integrals (11) and (12) are negligible.

Equations (11) and (12) may be compared to Cormack's more compact result[11]

$$\rho_m(p) = -\frac{1}{\pi} \int_{|p|}^\infty \frac{dg_m(p_z)}{dp_z} \frac{T_m(p_z/p)p\, dp_z}{(p_z^2 - p^2)^{1/2}}\,. \quad (13)$$

Equation (13) is actually equivalent to Eqs. (11) or (12) if m is even or odd, respectively.[16] This can be shown as follows. For Eq. (11) and (12) express the integration in the $p_z < p$ range as an integral over a Chebychev polynomial of the second kind and the integration in the region $p_z > p$ as an integral over a linear combination of a Chebychev polynomial of the first kind and a Chebychev polynomial of the second kind. The two integrals over the polynomial of the second kind can be combined into one integral from $p_z = 0$ to ∞. From the properties of the $g_m(p_z)$ functions[11] this integral must vanish.[16] This leaves the integral over $T_m(p_z/p)$ in the $p_z > p$ range which is just Eq. (13).

One of the properties which the $g_m(p_z)$ functions must satisfy in order to be able to carry out the manipulations described in the previous paragraph is that they must fall off faster than $p_z^{-(m+1)}$ for large-p_z values.[11] This is necessary in any of the integrals in which the $g_m(p_z)$ function or its derivative is combined in the integral with a polynomial. However, as pointed out by Cormack,[16] in practice

the $g_m(p_z)$ functions obtained from real data rarely satisfy all the required properties. It is a distinct advantage of our formulation of the solution that the derivatives $dg_m(p_z)/dp_z$ are never combined with polynomials in the integral in such a way that they must obey stringent requirements, like falling off as $p_z^{-(m+1)}$ for large p_z. In fact the integral will always consist of the function dg_m/dp_z combined with a function which itself falls off as $p_z^{-(m+1)}$.

We can now explore the consequences of certain symmetries in the $\vec{p}$-space plane in which the analysis is being done. If the momentum distribution $\rho(\vec{p})$ is symmetric with respect to reflection about some axis then we may choose this axis as our reference axis, ζ in Fig. 1. This means that $\rho(p,\phi) = \rho(p,-\varphi)$ from which it follows that $\rho_m(p) = \rho_{-m}(p)$. This, combined with the reality condition, means that $\rho_m^i(p) = 0$, i.e., $[\rho_m(p)]$ are real for all m. Thus $[g_m(p) | m = 0,1,2,\ldots]$ are real and n data sets $[N_{\alpha_j}(p_z)]$ now determine n $\rho_m(p)$ functions [compare this to the general case of no symmetry when we can only determine $\frac{1}{2}(n+1)$ complex coefficients, for n odd].

If rather than just reflection symmetry we have a fourfold rotation symmetry then only terms for which $m = 4l$, l an integer, will be nonzero in general. This results in

$$\rho_{4l}(p) = \frac{-1}{\pi}\int_0^\infty dp_z \frac{dg_{4l}(p_z)}{dp_z} \times \begin{cases} \dfrac{\sin[4l \arcsin(p_z/p)]}{(p^2 - p_z^2)^{1/2}}, & p_z < p \\ \dfrac{p^{4l}}{(p_z^2 - p^2)^{1/2}[p_z + (p_z^2 - p^2)^{1/2}]^{4l}}, & p_z > p . \end{cases} \tag{14}$$

This is the symmetry which exists in the (001) p-space plane of systems with cubic symmetry. Equation (14) will be used in Sec. IV to analyze Cu data taken in the (001) plane.

Finally if the distribution is isotropic, we have $\rho_m(p)$ for $m > 0$, which leaves

$$\rho(\mathrm{p}) = \rho_0(p) = \frac{-1}{\pi}\int_{|p|}^\infty dp_z \frac{dg_0(p_z)}{dp_z}(p_z^2 - p^2)^{-1/2} . \tag{15}$$

Equation (15) will be used to analyze the hypothetical free-electron data in Sec. III.

III. APPLICATION TO A HYPOTHETICAL FREE-ELECTRON CASE

In order to get some feel for the effects of discontinuities in $\rho(p)$, statistical errors in $N_\alpha(p_z)$ data, and finite resolution of experimental apparatus on the reconstruction of $\rho(p)$ from the $N_\alpha(p_z)$ data the hypothetical case of a free-electron metal with a Gaussian-core contribution to $\rho(p)$ was used to generate "data," $N_\alpha(p_z)$. The choice of functional form for the momentum density was

$$\rho_f(p) = 0.125\Theta(p_f - p) + \frac{1}{(\pi a)^{1/2}} e^{-p^2/a^2} . \tag{16}$$

Here p_F was taken to be 5 mrad, a was chosen to be 9.608 98 mrad^2 and $\Theta(p_F - p)$ is the step function. This generated "data" of the form

$$N(p_z) = 0.25(25 - p_z^2)^{1/2}\Theta(p_F - p_z) + e^{-p^2/a^2} , \tag{17}$$

where we have dropped the α subscript since this is an isotropic situation. Data points were calculated at 0.25-mrad intervals from Eq. (17) for $p_z = 0$ to 20 mrad. This then represented data taken from a free-electron metal without statistical error with an experimental apparatus with infinitely fine resolution.

A general computer program was written to calculate $[g_m(p_z)]$ from $[N_\alpha(p_z)]$ and to numerically integrate Eq. (14). $g_m'(p_z)$, the first derivative of $g_m(p_z)$ with respect to p_z was calculated by fitting $g_m(p_z)$ to a second-degree polynomial, locally, at three consecutive points. The program was then applied to the data generated from the free-electron case above.

Figure 2(a) shows the original $\rho_f(p)$ from Eq. (16). Figure 2(b) shows the reconstructed momentum density. The overall agreement is exceedingly good with the exception of the small peak in Fig. 2(b) around 5 mrad. The origin of this can be directly traced to the calculation of $g_0'(p_z)$. For this case, which is isotropic, $g_0(p_z) = N(p_z)$ and $g_m(p_z) = 0$ if $m > 0$. Since $g_0'(p_z)$ is calculated from a local polynomial fit and since the actual derivative at $p_z = p_F$ is infinite, the values of $g_0'(p_z)$ calculated for $p_z \leq p_F$ become larger (i.e., less negative) than the actual derivatives of $N(p_z)$ near to but less than p_F. Hence, the integral contributes larger values near the p_F to the reconstructed $\rho(p)$ than would be expected. Artifacts, like this, which result from discontinuities in derivatives of $[g_m(z)]$ are sensitive to the method of calculation of $[g_m'(z)]$. The reason that local deviations like this are kept localized and not smeared out by the integration of Eqs. (14) and (15) is made clear in the error analysis which follows.

In order to study the effect of statistical errors in $N_\alpha(p_z)$ on the reconstruction of $\rho(p)$, various points in the previously generated data, $N(p_z)$,

for the free-electron case were increased by a fixed amount ΔN for various p_z values: 0.5, 2, 6, and 10 mrad. ΔN amounted to a 5% error in "count rate" in the hypothetical data near $p_z = 0$. Of course it amounted to a much larger percentage error at $p_z = 10$ mrad, but in general a large percentage error will occur at larger angles where count rates are lower and fewer counts are taken. Figure 2(c) shows the superpositron of the four $\rho(p)$ functions calculated from the four sets of data, each with an error at a different point. An interesting observation is that although ΔN represented a smaller percentage error in the data at $p_z = 0.5$ mrad than at any other point, it generated one of the largest percentage errors in $\rho(p)$ of the four error points involved. The reason for this can be seen in the integral in Eq. (15). Let us break the integration into two regions $p \to p + \Delta P$ and $p + \Delta P \to \infty$, where ΔP represents the extent of the region of points used to locally fit $g_0(p_z)$ to a polynomial, i.e., it is the local region in which an error in $N_\alpha(p_z)$ produces the largest effects in $g_0'(p_z)$.

The first integration becomes

$$\int_p^{p+\Delta P} dp_z \, \frac{g_0'(p_z)}{(p^2 - p_z^2)^{1/2}} . \tag{18}$$

From the mean-value theorem there exists an "average" value, $\bar{g}_0'(p_z)$ such that we can write

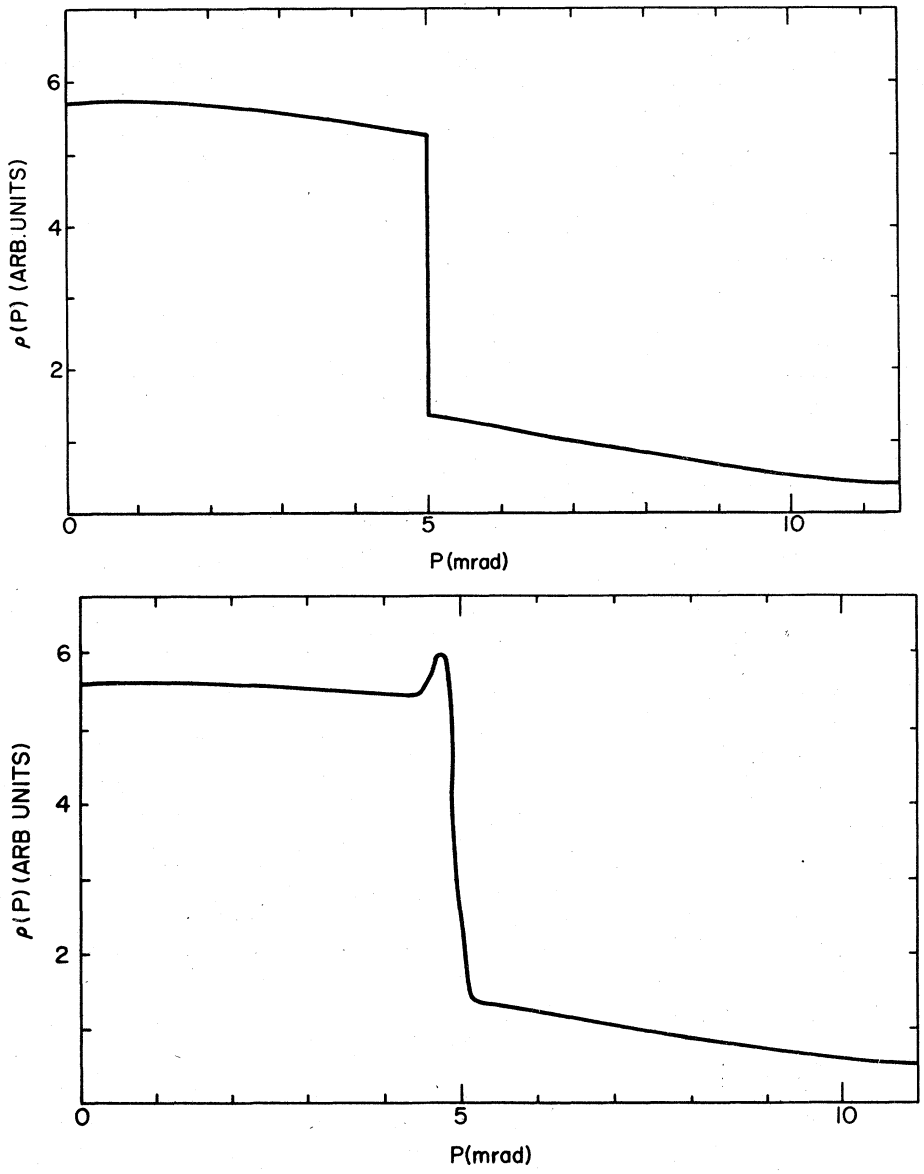

FIG. 2 (a) Theoretical free-electron distribution. (b) Reconstructed free-electron distribution using the "data" generated by Eq. (12). (c) Superposition of four reconstructed distributions each reconstructed from data with an error of +5% of the $N(p_z = 0)$ value introduced at one point.

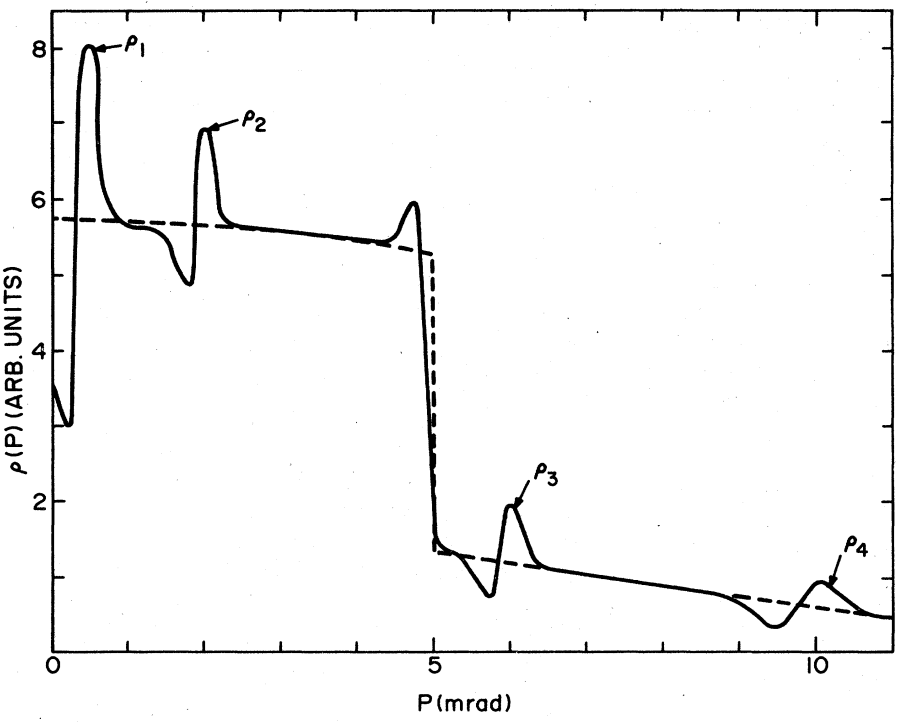

FIG. 2. (*Continued*)

Eq. (18) as

$$\bar{g}_0'(p_z)\int_p^{p+\Delta P}\frac{dp_z}{(p^2-p_z^2)^{1/2}}\ . \tag{19}$$

Integrating Eq. (19), we have

$$\bar{g}_0'(p_z)\ln[(1/p)(p+\Delta P)^2-p^2)]\ . \tag{20}$$

Now, for $p<p_F$ $\rho(p)$ is nearly constant and the integral in Eq. (15) is nearly p independent. However, Eq. (20) shows that the integration region near $p_z=p$ contributes more and more to the total integral in Eq. (15) as $p\to 0$. It is in fact divergent at $p=0$. Thus small changes in $N_\alpha(p_z)$ becomes magnified near $p_z=0$. In general, Eq. (18) controls the overall integral Eq. (15), especially for small-p values. The situation in the particular case of positron annihilation where $N_\alpha(p_z)$ and thus $g_m(p_z)$ are nearly flat for small-p values is conductive to generation of oscillations like those in Fig. 2(c). Small changes in $N_\alpha(p_z)$, and thus in $g_m(p_z)$, in a nearly flat region produce changes of sign in $g_m'(p_z)$ which are magnified by the integration and appear as oscillations around the local mean value of $\rho(p)$. However, because these variations manifest themselves through local changes in $g_m'(p_z)$, if $g_m'(p_z)$ is on the average zero over the entire region of integration the result will not show the effect of the variation. This happens, for example, when there is a small "bump" in $g_m(z)$ as in the induced errors in the free-electron case. This explains why the induced errors did not affect $\rho(p)$ at points far from the error points. It was only when the integration was over part of the error region that $g_m'(z)$ was not zero on the average and large contributions to $\rho(p)$ resulted.

The propagation of errors, that is data points that fall outside a smooth curve drawn through the surrounding data points, can be put on a more intuitive level. The difficulties can be traced to the fact that the experiment is carried out in a manner perfectly described by Cartesian coordinates, whereas the reconstruction of $\rho(p)$ is done using a limited number of terms in a polar-coordinate expansion, i.e., the momentum density distribution is implicitly assumed to not have rapid variations with angle. We first examine the reasons that local changes in $N_\alpha(p_z)$ at say $p_z=p_0$ (e.g., statistical errors) result in local changes in $\rho(\vec{p})$ at $p=p_0$.

Since $N_\alpha(p_z)=\int\rho(\vec{p})\,dp_x$ we see that $p_z\leq p$ and thus the values $\rho_m(p)$ for $p<p_z$ cannot possibly account for any behavior in $N_\alpha(p_z)$. We may now ask why the values of $\rho(\vec{p})$ for $p\gg p_0$ are not affected. $\rho(\vec{p})$ is integrated along a straight line in the plane to generate $N_\alpha(p_z)$. If $\rho(\vec{p})$ is to "generate" the existing errors in $N_\alpha(p_z=p_0)$ then somewhere along the line of integration $\rho(\vec{p})$ must contain errors. However, if these are not near

$p = p_0$ then they lie further out in the plane along the line of integration at some angle α' with respect to the ξ axis (reference axis) and at some distance p_1, say, from the origin. But since we are using a limited number of terms in our Fourier expansion, there are no high-frequency components and the error could decay only slowly from around α' as a function of θ. For large values of p_1 this would imply that $N_\alpha(p_z)$ would detect the "error" for $p_z = p_0$, and the "error" in $N_\alpha(p_z)$ would fall smoothly with p_z. But this is not consistent with out original hypothesis that there is a single datum point abruptly out of line with nearby data. Thus the error in $\rho(p)$ must appear at $p \cong p_0$ if the error in $N_\alpha(p_z)$ appears at $p_z = p_0$.

The magnification of errors as $\vec{p} \to 0$ can be understood as follows. Lines of constant $\rho_m(p)$ are circles in the plane of integration. An error in $N_\alpha(p_z = p_0)$ generates errors in $\rho_m(p)$ in a region δp about $p = p_0$. Thus the error is confined to a circular band of width δp centered on the circle of radius $p = p_0$. Then to a rough approximation the error in $N_\alpha(p_z = p_0)$ is given by

$$\Delta N \sim \Delta\rho l ,$$

where $\Delta\rho$ is the associated error in $\rho(\vec{p})$ and l is the length of the line of integration intersecting the circular error band. For $\delta p \ll p$ the angle ϕ subtended by the chord l varies as $p^{-1/2}$. However, $l = \phi p$ and we have

$$\Delta\rho \sim \Delta N / p^{1/2} .$$

The errors induced in $\rho(\vec{p})$ by ΔN vary inversely as $p^{1/2}$. Or, in words, for a fixed ΔN, as p becomes smaller the region of integration which covers the error in $\rho(\vec{p})$, $\Delta\rho$, becomes smaller and larger values of $\Delta\rho$ are required to cause the same percentage error in $N_\alpha(p_z)$. The same analysis applied to reconstruction of $\rho(\vec{p})$ from long-slit data yields the result

$$\Delta N \sim \Delta\rho\Omega p^2 ,$$

where Ω is the solid angle subtended by the area of integration over the error region $\Delta\rho$. For $\delta p \ll p$, $\Omega \sim 1/p$. Thus for long-slit reconstruction

$$\Delta\rho \sim \Delta N / p$$

and the errors vary as p^{-1}. This is the reason errors in long-slit data produce so much larger errors in the reconstruction of $\rho(\vec{p})$ as $p \to 0$ than occur for the reconstruction of $\rho(\vec{p})$ from point-geometry data.

Finally, the effect of finite resolution on the reconstruction of $\rho(p)$ was investigated. The theoretical free-electron data, $N(p_z)$, was averaged locally in a manner which reflected the finite resolution of our experimental set up. This had the effect of smearing the $N(p_z)$ function and thus also $\rho_f(p)$ into a function which is shown as the dashed line in Fig. 3 [compare with Fig. 2(a)], i.e., this is the best that could be hoped for in the reconstruction of $\rho(p)$ from the smeared data. The solid line in Fig. 3 shows the reconstructed $\rho(p)$. The reconstruction agrees very well with the smeared $\rho(p)$ function showing that the method can correctly reconstruct $\rho(p)$ providing the errors are kept small and there are no discontinuities in derivatives in the data. The small differences between the two functions in Fig. 3 near $p = 0$ are due to not using enough significant figures in the original smeared $N(p_z)$ data.

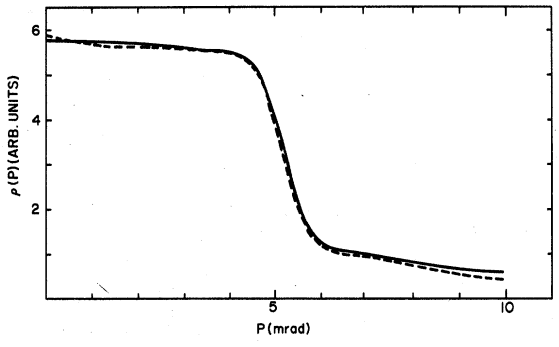

FIG. 3. Reconstructed $\rho(p)$ (solid line) using smeared data as compared to actual smeared $\rho(p)$ (dashed line).

IV. APPLICATION TO REAL DATA

Data were taken using an apparatus conceptually quite different from those used previously to achieve the crossed slit geometry.[17-21] In particular it is designed around two unique γ-ray collimators each consisting of an array of 210 tantalum tubes (with dimensions 40×0.040 in. with a 0.002-in. wall) aligned parallel to within 0.001 in. along their entire length. These provided an angular resolution of approximately 0.9 mrad in two directions independent of sample size or sample to γ-ray detector distance. The collimators are mounted on machined aluminum I beams which are articulated by a "vertical feed" machine tool driven by a stepping motor. The detectors are Tl-activated NaI (dimensions of 3 in. diameter by 4 in. long) interfaced with conventional coincidence counting electronics. A more detailed description of the apparatus and its performance is being prepared.[22]

Data were taken in various crystallographic directions including the (001) p-space plane of copper with p_z in the [110] and [100] directions. A

total of 40 000 coincidence counts were accumulated each 0.25 mrad out to 4.5 mrad falling to 8000 counts at 7.0 mrad. Approximately 15% of the counts were accidental. Beyond 7.0 mrad data was taken every 0.5 mrad. These data were used to reconstruct $\rho(p)$ in the (001) plane. Although we can use only two terms in the Fourier series to reconstruct $\rho(p)$ in the (001) plane using Eq. (14), a surprising amount of detail emerges. Figure 4 shows the results of the reconstruction for $\rho(p)$ in the [100] and [110] directions using essentially raw data which have only been normalized to have the same areas. It can be seen that even without smoothing the data, $N_\alpha(p_z)$, $\rho(p)$ can be reconstructed for $p<p_F$, the Fermi radius, without the errors becoming overwhelming. This is not the case for reconstruction of $\rho(p)$ from long-slit data in which even smoothing of the data will not remove the wild oscillations which occur in $\rho(p)$ for $p<p_F$. If we smooth the (001) data by a least-squares local parabolic fit to seven points, a subsequent reconstruction yields Fig. 5, which is quite well behaved everywhere except for $p<1$ mrad. These reconstructions should be compared with Fig. 6 which shows, qualitatively, the trends in $\rho(p)$ in the [110] and [100] directions as calculated by Mijnarends[14] using a Korringa-Kohn-Rostoker-Ziman method. The smaller Fermi radius of the [110] direction is clearly reproduced. However, the most impressive results are in the reproduction of the anisotropies beyond $p=5$ mrad. This substantiates the claim formerly made that the reconstruction of $\rho(p)$ in a plane requires less data when the point geometry setup is used. For example, Mijnarends required data in 6–8 directions in his analysis of long-slit data to show the same anisotropies in the [100] and [110] directions.

At this point we should remark on the differences

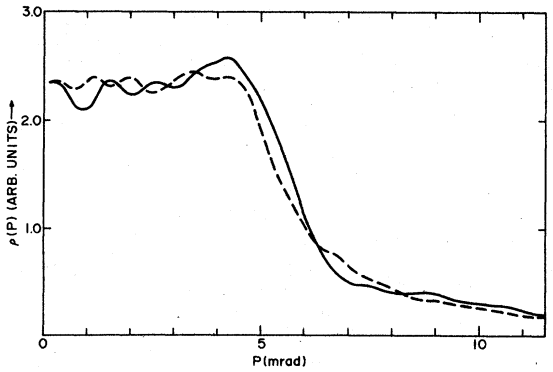

FIG. 5. Reconstruction of $\rho(p)$ as in Fig. 4, but from smoothed data.

in apparent Fermi radius, p_F, for the two directions [100] and [110]. While de Haas–van Alphen results [23,24] show that the difference $p_F([100]) - p_F([110]) \approx 0.5$ mrad, we see that this is not the case for the reconstruction, $\rho(p)$ in which $p_F([100]) - p_F([110]) \approx 0.25$ mrad. Mijnarends in his reconstruction of $\rho(p)$ also found this discrepancy in p_F for these two directions. The explanation is easily seen from Fig. 6. Although $\rho(p)$ has been reconstructed we have not eliminated the effects of finite resolution. Thus the $\rho(p)$ we have calculated is actually a smeared momentum distribution. We can get a good feeling for the effects of the finite resolution on the reconstructed momentum density $\rho_{\text{rec}}(p)$ as it related to the "true" momentum density for values of $p \gg \Delta$, the half-width of the resolution function. We first write

$$\rho_m(p) = \frac{1}{p} \int_0^\infty dp_z \frac{dg_m}{dp_z} F\left(\frac{p_z}{p}\right),$$

where $F(p_z/p)$ is the appropriate integrand for

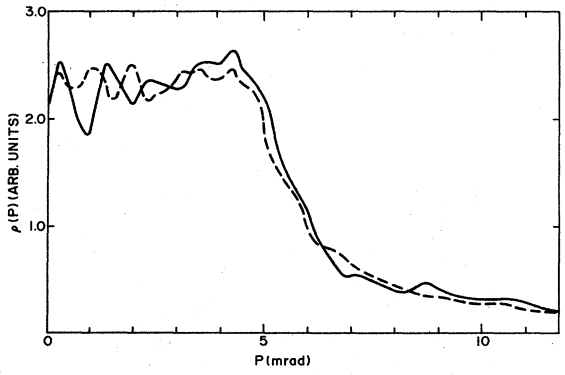

FIG. 4. Reconstructed $\rho(p)$ along [100] (solid line) and [110] (dashed line) directions for pure copper.

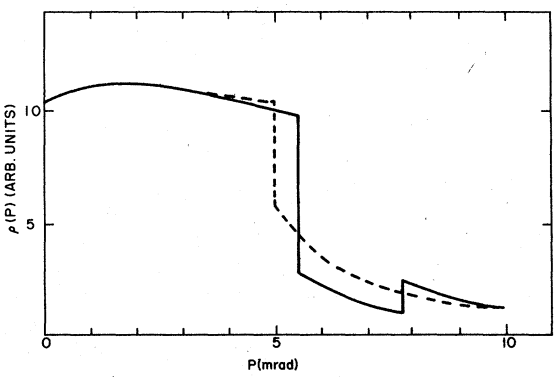

FIG. 6. Qualitative theoretical variation of $\rho(p)$ along [100] (solid line) and [110] (dashed line) following Mijnarend's calculation (Ref. 14).

the mth term into which all constants have also been absorbed. The function $g_m(p_z)$ is related to the "true" profile Fourier coefficients $h_m(\xi)$ by

$$g_m(p_z)=\int r(\xi)h_m(\xi+p_z)\,d\xi\ ,$$

where $r(\xi)$ is the resolution function. We can substitute the above integral over $h_m(\xi+p_z)$ for $g_m(p_z)$ in the $\rho_m(p)$ equation and interchange the order of the integrations, thus

$$\rho_m(p)=\int d\xi\, r(\xi)\frac{1}{p}\int_0^\infty dp_z\,\frac{dh_m(\xi+p_z)}{dp_z}F\left(\frac{p_z}{p}\right)\ .$$

We now want to transform this into an equation which relates the smeared coefficient $\rho_m(p)$ to the Fourier coefficient σ_m of the true momentum distribution. We can do this as follows. We first suppose that $r(\xi)$ gives contributions only in a region of size Δ and p_z and that we are interested only in the range $p \gg \Delta$. We may then approximate p by $p+\xi$ and p_z by $p_z+\xi$ in the above double integral. The first integration then equals the true mth coefficient $\sigma_m(\xi+p)$ as determined from $h_m(\xi+p_z)$. We can then write

$$\rho_m(p)\approx\int d\xi\, r(\xi)\sigma_m(\xi+p)\ .$$

Since σ_m is the true mth coefficient of the momentum distribution, substitution of the last equation into the polar series expansion for $\rho(p)$ yields

$$\rho_{\rm rec}(p)=\int r(\xi)\rho(\xi+p)\,d\xi\ ,$$

where $\rho_{\rm rec}(p)$ is the reconstructed momentum distribution, $r(\xi)$ is a function which represents the finite resolution of the experimental apparatus, and $\rho(p+\xi)$ represents the actual momentum distribution. In our case we are interested in $p \gtrsim 5$ mrad and our resolution yields a Δ of about 0.5 mrad so that the above approximation should be adequate for our purposes.

Thus we see that $r(\xi)$ smears out the Fermi surface and, what is important to this discussion, gives contributions to $\rho_{\rm rec}(p)$ from states just beyond p_F when $p<p_F$. This would not matter if all core states beyond p_F had the same $\rho(p+\xi)$ value but, as can be seen from Fig. 6, the core contributions for various directions differ. It is the larger core contribution in the [110] direction which makes p_F ([110]) appear to be larger, relative to p_F ([100]), than it really is.

To illustrate this further we have smeared Fig. 6 by using for $r(\xi)$ a Gaussian with full width at half maximum equal to 1 mrad, approximately our experimental resolution. Figure 7 shows the resulting distribution. The effect on $p_F([100])-p_F([110])$ is as predicted. This shows that great care must be taken in analyzing positron-annihilation data and Compton-profile data for details of the Fermi surface. In particular it would seem that conclusions regarding Fermi radii cannot be made without some knowledge of the core states just beyond p_F.

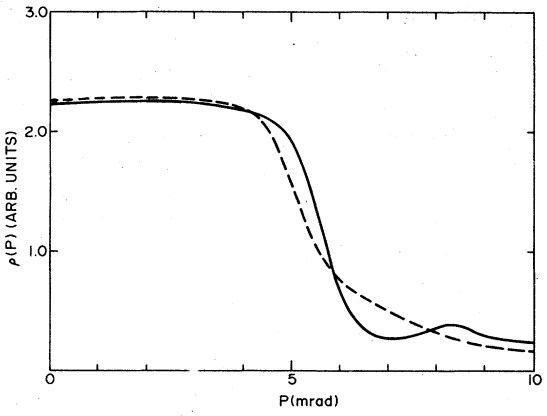

FIG. 7. Result of smearing Fig. 6 with a finite resolution according to Eq. (16). Note that the difference in apparent Fermi radii does not match the difference between the curves in Fig. 6.

We see also that Fig. 7 agrees quite nicely with Figs. 4 and 5 in overall shape. The only major differences (disregarding oscillations due to statistical errors below $p=3$ mrad) are the humps in the distribtuions of Figs. 4 and 5 from ~3.5–~5 mrad for both directions. These may be the result of many-body effects[25] which are predicted to cause peaks in $\rho(p)$ near p_F. If so it would appear that these effects are anisotropic since near $p=5$ mrad $\rho(p)$ for [110] is predicted to be slightly larger than $\rho(p)$ for [110] (see Fig. 6), but the reconstructions, Figs. 4 and 5, show just the opposite.

V. SUMMARY

We have presented a method for generating $\rho(\vec{p})$ in a plane from crossed-slit positron-annihilation data taken in the same plane. Analysis of error propagation showed that the errors in $\rho(\vec{p})$ generated by errors in the data are generally not as severe as with the reconstruction of $\rho(\vec{p})$ from long-slit data. Thus if one is interested in $\rho(\vec{p})$ for a few selected directions the point geometry set up would be preferred for the acquisition of data for reconstruction of $\rho(\vec{p})$. In addition by choosing the plane of highest symmetry contain-

ing the desired directions it is possible to eliminate many of the unknown Fourier coefficients and thus obtain $\rho(\vec{p})$ effectively to many more terms from the same amount of data.

The application of the method to Cu data taken in the (001) plane was presented as illustrative of the method. Using only two sets of data taken for two different crystal orientations we were able to reconstruct $\rho(\vec{p})$ and investigate a large number of details regarding the difference in $\rho(\vec{p})$ in the [100] direction compared to the [110] direction in extended P space. The particular application to Cu also pointed out the pitfalls which occur when determination of various quantities like p_F are attempted. Namely, one must take into consideration the resolution function of the experimental apparatus and certain details of $\rho(\vec{p})$ around the region of interest before quantitative conclusions can be drawn. This information (such as the relative magnitude of higher-momentum components in the vicinity of the Fermi surface) will not, in general, be available from other sources but rather falls naturally and automatically out of this procedure of calculating $\rho(p)$.

Overall it may be concluded that positron annihilation can be employed to generate realistic $\rho(\vec{p})$ functions for metals and that the point-geometry experimental method enjoys the distinction of requiring less data and being more accurate than the long-slit method for obtaining $\rho(\vec{p})$ in particular directions.

ACKNOWLEDGMENTS

We should like to thank H. Davis for the able execution of his many responsibilities contributing to the collecting of our positron-annihilation data. We should like also to express our appreciation for the cooperation of T. Raby and his "reactor operations" group at the National Bureau of Standards nuclear reactor—in particular N. Bickford. We are indebted to C. Vold of NRL for his help in the crystallographic orientation of the Cu single crystal and to Dr. J. T. Schriempf for his sustained support and encouragement of this work. One of us (L.P.) would like to acknowledge the support of the National Research Council through an NRC-NRL postdoctoral Associateship.

[1]R. A. Crowther, D. J. DeRosier and A. Klug, Proc. R. Soc. A 317, 319 (1970).
[2]R. N. Bracewell, Aust. J. Phys. 9, 198 (1956).
[3]A. Klug and R. A. Crowther, Nature (Lond.) 238, 435 (1972).
[4]C. K. Majumdar, Phys. Rev. B 4, 2111 (1971).
[5]C. D. Malonado, J. Math. Phys. (N. Y.) 8, 230 (1967).
[6]P. E. Mijnarends, Phys. Rev. 160, 512–519 (1967).
[7]P. E. Mijnarends, Phys. Rev. 178, 622–629 (1969).
[8]G. Kontrym-Sznajd and J. Stachowiak, Appl. Phys. 5, 361–365 (1975).
[9]T. Pajak, St. Charbik, B. Rozenfeld, and G. Kontrym-Sznajd, Acta Phys. Pol. A 50, 623–632 (1976).
[10]A. Cormack, J. Appl. Phys. 34, 2722 (1963).
[11]A. Cormack, J. Appl. Phys. 35, 2908 (1964).
[12]A. Cormack, Phys. Med. Biol. 18 195–207 (1973).
[13]R. A. Brooks and G. diChiro, Phys. Med. Biol. 21, 689 (1976).
[14]P. E. Mijnarends, Physics (N. Y.) 63, 235–247 (1973).
[15]J. S. Gradshteyn and I. M. Ryzik, *Tables of Integrals, Series and Products* (Academic, New York, 1965).
[16]A. Cormack (private communication).
[17]S. Berko and J. Mader, Appl. Phys. 5, 287 (1975).
[18]P. Colomkino, B. Fiscella, and L. Trossi, Nuovo Cimento 27, 589 (1963).
[19]E. H. Becker, A. G. Gould, E. M. D. Senicki, and B. G. Hogg, Carr. J. Phys. 52, 336 (1974).
[20]M. Haseguwa, T. Suzuki, and M. Hirabayashi, J. Phys. Soc. Jpn. 37, 85 (1974).
[21]K. Fujiwara and O. Sueoka, J. Phys. Soc. Jpn. 21, 1947 (1966).
[22]A. Ehrlich (unpublished).
[23]E. I. Zornberg and F. M. Mueller, Phys. Rev. 151, 557 (1966).
[24]A. S. Joseph, A. C. Thorsen, E. Gertner, and L. E. Valby, Phys. Rev. 148, 569 (1966).
[25]S. Kahana, Phys. Rev. 117, 123 (1960).